Simulation of Toner Particle Movement between a Cylindrical OPC and Developer

Jang Yi, Everett, MA USA

Abstract

A calculation procedure for 2D simulation of toner particle movement between a cylindrical OPC and a cylindrical developer in the presence of an AC bias is presented. The potential between two flat surfaces is calculated using the finite element method with its initial potential analytically calculated incorporating contributions from toner particles whose internal charge distribution is approximated with a cosine pulse. The flat surface potential is then transformed into the physical geometry using conformal mapping techniques and the corresponding electric field is obtained by interpolating the potential and taking its spatial differences. Toner movement between the two rotating, cylindrical surfaces due to the force field is calculated using the discrete element method.

Simulated particle movement data using various line widths and AC bias settings are analyzed to qualitatively explain developed line width gain variations. Simulated single line development shows a larger line width gain than thicker lines. It is observed that particle movement around the exposed region begins to stabilize at a certain rotation angle of the exposed region, which appears to be correlated with the input line width dependent line width gain variation. An increase in AC bias magnitude and a decrease in AC bias frequency tend to exacerbate the line width gain variation.

Introduction

Non-contact, mono-component development systems transport toner particles by creating an alternating electric field between two rollers during the development process. Although the fundamental mechanism for such phenomenon is straightforward, more detailed aspects such as dot gain variation with varying development parameters are not fully understood and most of the theoretical work in toner movement has been limited to stationary surfaces and much simplified geometry involving flat donor/receptor surfaces. In this paper, toner movement in a realistic 2D setting with cylindrical, rotating surfaces is investigated and simulation data are analyzed to give a reasonable explanation for line width gain variations.

Nominal print engine parameters used in this work, unless noted otherwise, are given in Table 1.

Methodology

Dynamic motion of charged toner particles between two rotating rollers with equal radii is calculated based on the strength of electric field. The developer rotates clockwise and the OPC rotates counterclockwise. The electric field between the two rollers with numerous charged particles is not easily obtained. To overcome this calculation problem, the potential between two flat surfaces is first calculated and transformed into the physical geometry using conformal mapping techniques. The electric field is then obtained by interpolating the transformed potential and taking its spatial differences. Toner movement is iteratively calculated from the field using the discrete element method.

Table 1: Development Parameters

particle radius (R_t)	10 μm
developer radius	1 cm
OPC radius	1 cm
print speed	40 ppm
DC bias	–400 V
AC bias type	square wave
AC bias magnitude (V_{AC})	600, 1000 V
AC bias frequency (f_{AC})	500, 1000, 1500, 2000 Hz
dark voltage	–700 V
light voltage	–100 V
air gap (g)	250 μm
Δt	0.5 μs
Δx, Δy	5 μm
OPC thickness (d)	20 μm
OPC dielectric constant	3
toner dielectric constant (ε_t)	3
toner charge density distribution	log-normal (see Fig. 1)
laser power	0.3 mW
horizontal laser spot size	80 μm
vertical laser spot size	90 μm
laser beam rise and fall times	1 ns
print resolution	600 dpi

Toner movement is also affected by the particles' collisions with the mechanically rotating rollers and physical movement of the exposed region on the OPC surface. The former is embedded in the discrete element method and the latter is implemented by horizontally moving the exposed region in the parallel-plate coordinate system during each iteration.

Toner Charge Distribution

The toner charge density distribution is assumed to be log-normal, as illustrated in Fig. 1. The mean density is about -10 μC/cm^3 and the wrong signed toner takes up 1.2% of the population.

For mathematical convenience, suppose the volume charge density within each particle varies as follows

$$\rho_i(x,y) = \rho_{i,max} \times \begin{pmatrix} \cos(\omega_0(x-x_i))[u(x-x_i+R_t)-u(x-x_i-R_t)]\times \\ \sin(\omega_0(y-y_i+R_t))[u(y-y_i+R_t)-u(y-y_i-R_t)] \end{pmatrix} \quad (1)$$

where i is the particle number, $\rho_{i,max}$ whose distribution is shown in Fig. 1 is the volume charge density at the center of the ith particle, R_t is the particle radius, $\omega_0 = \pi/(2R_t)$, and x_i and y_i are the x and y positions of the particle. $\rho_i(x, y)$ describes a 2D cosine pulse centered at (x_i, y_i) and is effectively utilized in the subsequent analytic potential calculation.

Potential between Two Flat Surfaces

With N toner particles between two flat surfaces, as illustrated in Fig. 2, the potential in the gap is given by

$$\left(\frac{\partial^2}{\partial x^2}+\frac{\partial^2}{\partial y^2}\right)V(x,y) = -\sum_{i=1}^{N}\frac{\rho_i(x,y)}{\varepsilon_0\varepsilon_t} \quad (2)$$

where ε_t is the dielectric constant of the toner. The analytic solution of Eq. (2) can be obtained by taking the Fourier transform in the x direction and then Laplace transform in the y direction[1] and it consists of the potential V_{toner} due to the particles and the potential due to the OPC surface charge and developer bias. V_{toner} from a single particle in the middle of the gap along the y-axis with its maximum charge density set to −10 μC/cm^3 decays as the distance away from the particle increases in a similar way the voltage profile of a point charge attenuates, as illustrated in Fig. 3. The point charge potential was obtained by treating the particle as a point charge outside the particle and assigning a constant voltage $q_t/(4\pi\varepsilon_0 R_t)$ inside the particle (effectively making it a charged conductive sphere), where q_t = (−10 μC/cm^3) (4/3)πR_t^3. The point charge potential decays more rapidly around the particle and appears to level out sooner while V_{toner} actually reaches zero potential at the developer and the ground substrate. The two boundaries make V_{toner} change its shape and magnitude as the particles moves away from the middle of the air gap and gets closer to either boundary as shown in Fig. 4, where the y position of the particle ranges from 20 to 230 μm. Even though the analytic solution V_{toner} accurately describes the complex behavior of the potential due to a single particle, the actual implementation of it consists of a series of computationally expensive operations and its performance gets much worse with decreasing Δt since it needs to be calculated from scratch during each iteration. Thus, when the contributions from numerous particles at different locations are to be superimposed in such large scale geometry settings, it is very difficult to optimize it to a degree where tens of thousands of iterations can be performed within a reasonable amount of time on a desktop. Utilization of the point charge potential also raises performance issues since multiple image charges have to be introduced for each particle to satisfy the boundary conditions at both surfaces. For these reasons, the finite element method is utilized to run a set of simulations with varying parameters. The analytic solution with initial particle positions at the developer surface is used as the initial potential, which improved the first iteration performance by more than an order of magnitude compared to uniform initial potential in the gap. Except for the first iteration, the calculation time of the finite element method for a single iteration depends heavily on particle movement. The more the particles move, the longer it takes to calculate the potential with the finite element method. Thus, for a small Δt of 0.5 μsec used in this work, the finite element method performed significantly better than the analytic solution.

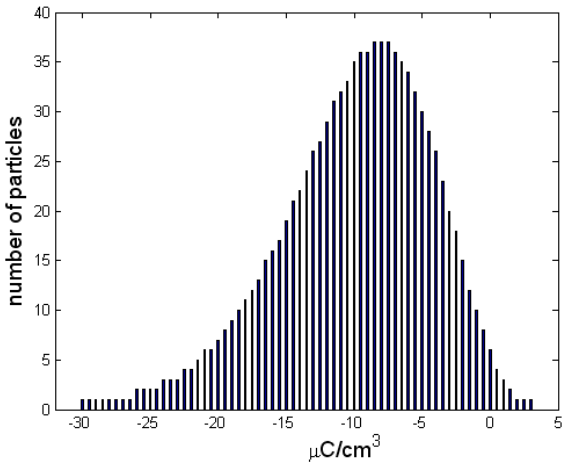

Figure 1. Toner charge density distribution

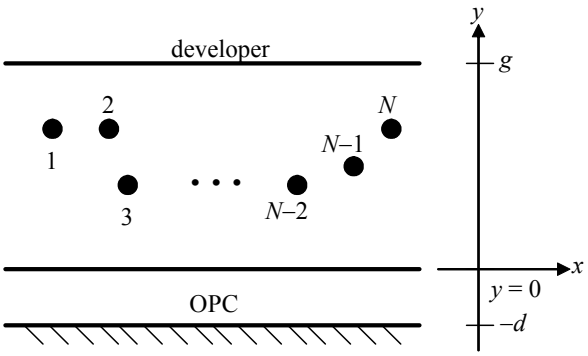

Figure 2. Parallel-plate coordinate system with N toner particles

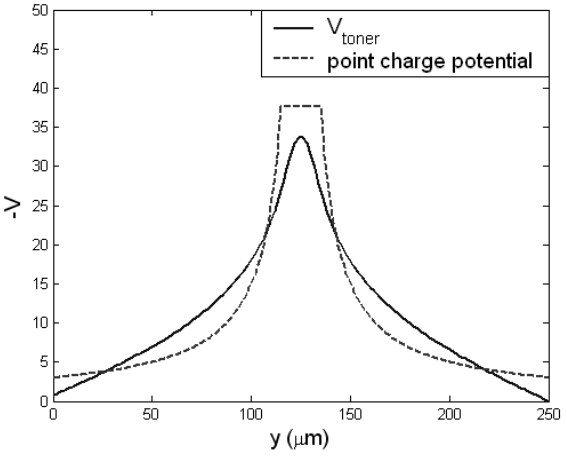

Figure 3. Potential along the y-axis

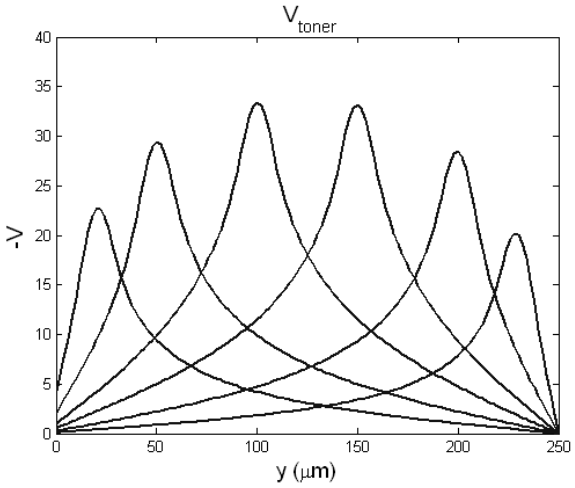

Figure 4. Potential along the y-axis with different y positions (20, 50, 100, 150, 200, and 230 μm) of the particle

Field between Two Cylindrical Surfaces

The potential in the gap discussed in the previous section is mapped onto the physical geometry with cylinders using conformal mapping techniques.[2] This is simply a mapping from one coordinate system to another and there is no modification of potential values during the process. As an example, the transformed potential of a 20-pixel wide line with toner particles adhering to the developer is shown in Fig. 5. Note that only long lines across the PC are considered for investigation since the mathematical development that started with Eq. (2) assumes that there is no potential variation in the direction perpendicular to the *xy*-plane (see Fig. 2). This requires that line widths be positive integer multiples of one pixel size, where each pixel represents a laser scan line.

After the transformation, each calculation cell is no longer rectangular, as illustrated in Fig. 6. The transformed potential is numerically interpolated to obtain the field at a given point. For example, the horizontal field at point **P** in Fig. 6 is set to $-(V_2-V_1)/\Delta x$, where V_1 and V_2 are computed in the parallel-plate coordinate system via bilinear interpolation.

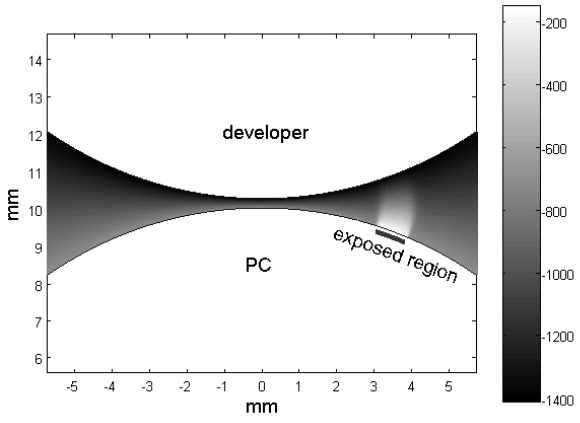

Figure 5. Transformed Potential

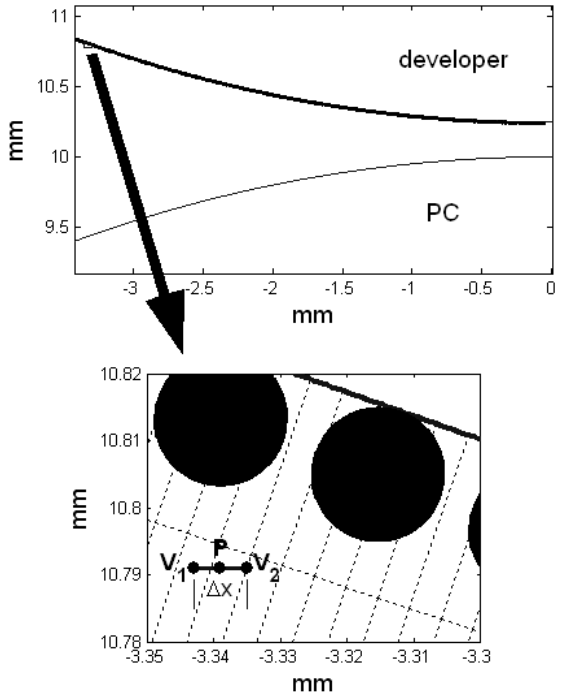

Figure 6. Potential interpolation. Transformed calculation cells are shown in dotted lines

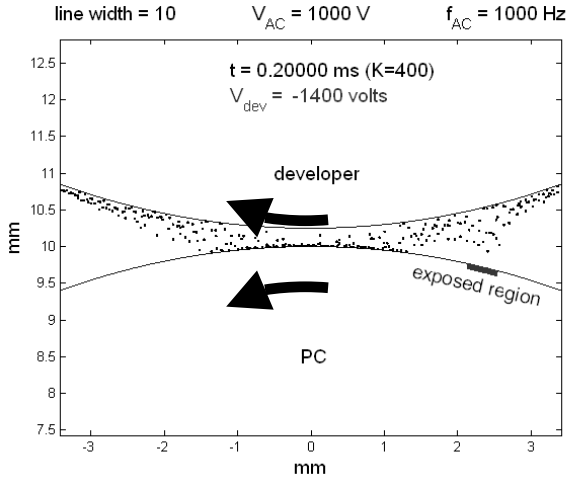

Figure 7. Toner movement

Toner Movement Calculation

For each particle, its motion in $\mathbf{z} = (x, y)$ is calculated with the following motion equation

$$m_t \ddot{\mathbf{z}} = q_t \mathbf{E} + \mathbf{F}_{contact} \tag{3}$$

where m_t is the particle mass, **E** is the field discussed in the previous section, and $\mathbf{F}_{contact}$ is the contact force from mechanical collisions with other particles and/or either roller surface and it is calculated using the discrete element method.[3]

Initially, there is one layer of toner particles adhering to the developer and the driving AC bias forces the particles to bounce back and forth between the two surfaces that rotate in the same direction, as shown in Fig. 7. OPC rotation is implemented by moving the exposed region $\Delta t \times$ (OPC rotation speed) in the parallel-plate coordinate system at the end of each iteration. The field and toner movement are then calculated based on the updated OPC surface charge.

In the rest of this paper, calculations in the right-half plane ($x > 0$) are omitted for performance improvement. This shouldn't affect the final development significantly since when the gap above the exposed region is very small, the polarity of the AC bias and the resulting normal field predominantly determine toner movement and particles can settle on the exposed region only after the gap begins to widen ($x < 0$).

Dynamic Development Quantization

The number of toner particles (N_d) that have been inside a virtual development region for at least one AC bias cycle and the corresponding line width (L_d) occupied by those particles are kept track of during each iteration to quantize development dynamics around the exposed region. The virtual development region is a non-rectangular box directly above the exposed region and its dimensions are shown in Fig. 8. When the gap above the exposed region is small, the AC bias with its alternating voltage will push the particles into the virtual development region, or pull them out of the virtual development region. As the gap gets larger, the number of particles inside the virtual development region begins to stabilize and less particles move in and out of the box.

The number of toner particles and line width in the virtual development region are recorded as a function of the development angle θ. θ represents the rotation angle of the exposed region (see Fig. 9). When θ reaches a certain point, L_d and N_d change little. This critical development angle θ_c is numerically obtained as the angle where the standard deviation of $L_d(\theta)$ for $\theta \geq \theta_c$ is less than 5 μm and it turns out be an important factor in line development, as discussed in the next section.

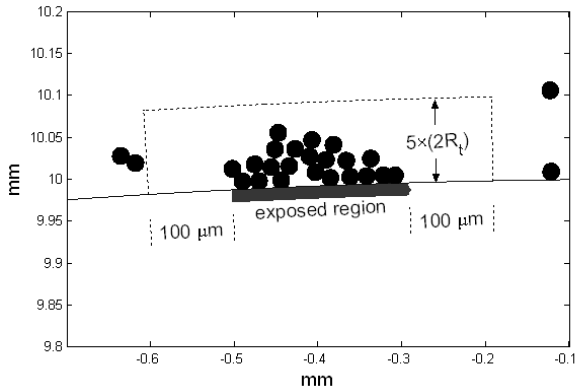

Figure 8. Virtual development region

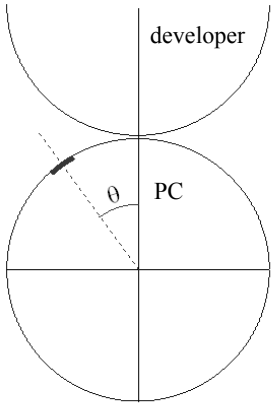

Figure 9. Development angle

Line Width Gain Variation

L_d of a single line with V_{AC} = 1000 V and f_{AC} = 1000 Hz is shown in Fig. 10 and it begins to stabilize around $\theta = 8°$. In comparison, L_d and N_d of a 10-pixel wide line with the same settings, shown in Fig. 11, continue to increase and fluctuate, so they do not appear to stabilize within the calculation range. When the AC bias magnitude is reduced down to 600 V, the critical development angles of the two lines are brought much closer to each other, as shown in Figs. 12 and 13. In both AC bias magnitude settings, the thin line seems to develop sooner than the thicker line. More importantly, the line width gain (developed width – original line width) from the single line is much larger than that from the 10-pixel wide line (a single 600 dpi dot is about 42 μm). This difference can be seen in snapshots shown in Figs. 14 and 15. For better visualization, the particles around the exposed regions are transformed into the parallel-plate coordinate system and they are shown in Figs. 16 and 17. The line width gain decreases as the input line width increases and an increase in AC bias magnitude seems to exacerbate the line width gain variation, as shown in Fig. 18. Also shown in Fig. 18 is the positive field width gain (positive field width – original line width) calculated in the parallel-plate coordinate system with g = 250 μm and V_{AC} = 0, which significantly underestimates the actual developed line width gain variation.

The critical development angle of the single line and the critical development angle variation as the line width increases appear to affect the line width gain variation (see Figs. 18 and 19). Even if the critical development angle changes little with varying input line width, the critical development angle of the single line and the corresponding effective air gap increase give rise to a noticeable line width gain variation. To illustrate this point, suppose that the critical development angle remains constant at 10° for the single and 10-pixel wide lines. The corresponding effective air gap is about 500 μm.[2] With two layers of uniformly charged toner (–10 μC/cm^3) developed, the electric field (calculated without the AC bias using the analytic method discussed in an earlier section) a few microns above the second layer for the two lines in the parallel coordinate system with an air gap of 500 μm is shown in Figs. 20 and 21. The particle diameter is adjusted to one half of the printer pixel for the sake of simplicity and the two layers cover the

exposed region plus one particle diameter on each end. The single line non-negative field width far exceeds the developed layer width. This indicates that more particles will be deposited around both ends, effectively increasing the development width. On the other hand, the non-negative field width of the 10-pixel wide line is actually smaller than the developed layer width. Thus, the final developed width gain won't exceed one printer pixel. This clearly verifies that an increase in air gap can result in a noticeable line width gain variation even if the critical development angle does not change with varying line width.

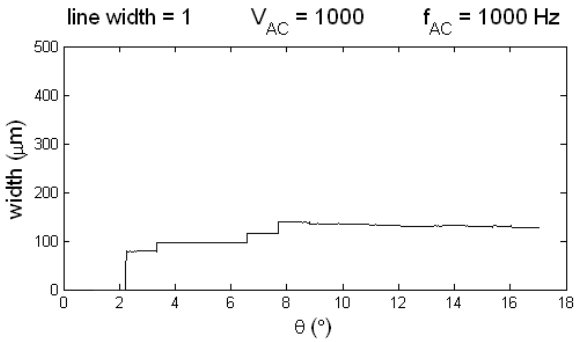

Figure 10. L_d of a single line

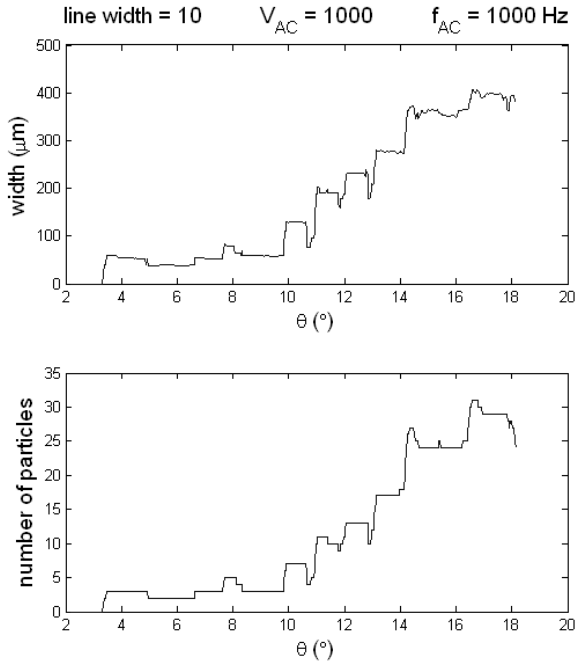

Figure 11. L_d (top) and N_d (bottom) of a 10-pixel wide line

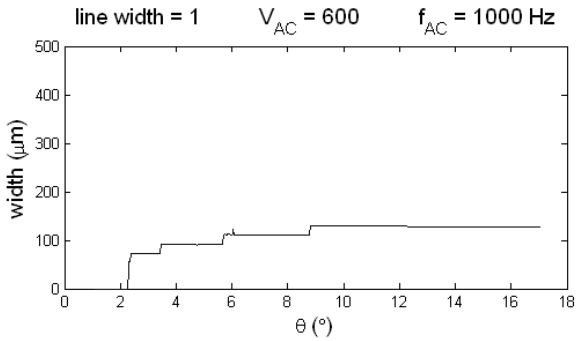

Figure 12. L_d (single line) when V_{AC} = 600 V

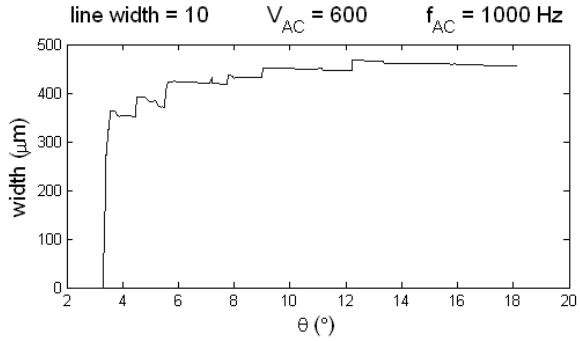

Figure 13. L_d (10-pixel wide line) when V_{AC} = 600 V

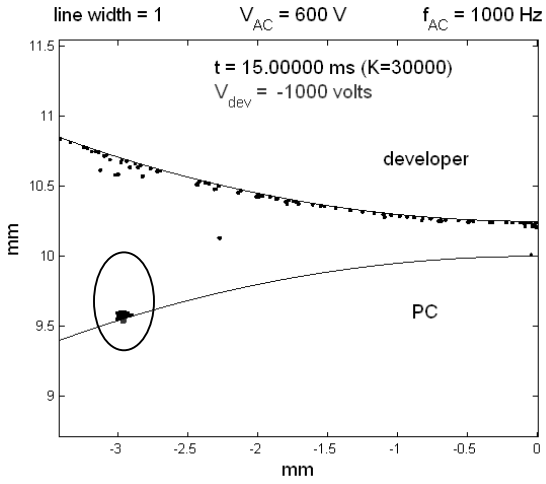

Figure 14. Single line development

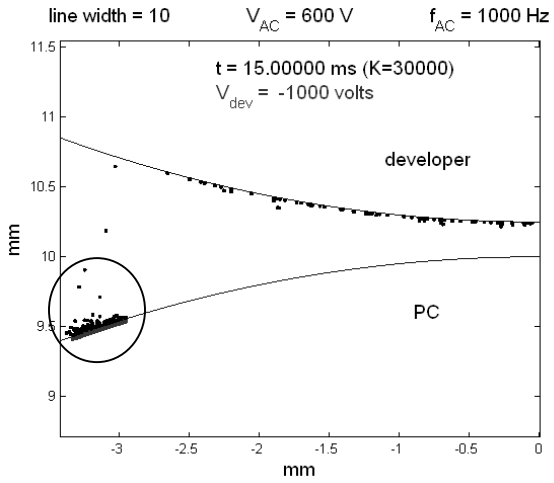

Figure 15. 10-pixel wide line development

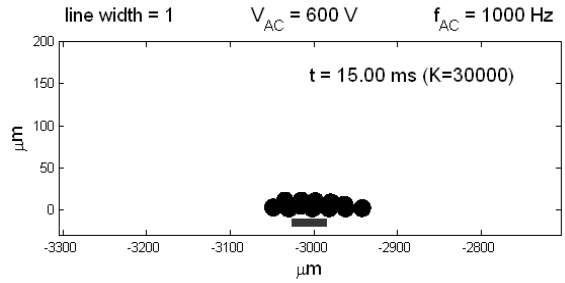

Figure 16. Particles above the exposed region in the parallel-plate coordinate system

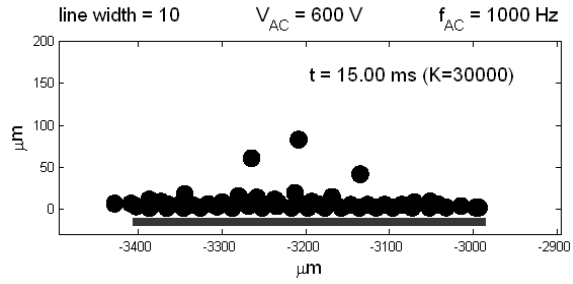

Figure 17. Particles above the exposed region in the parallel-plate coordinate system

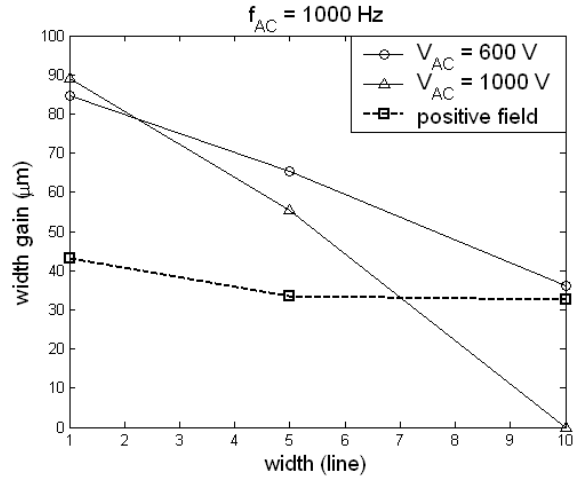

Figure 18. Line width gain

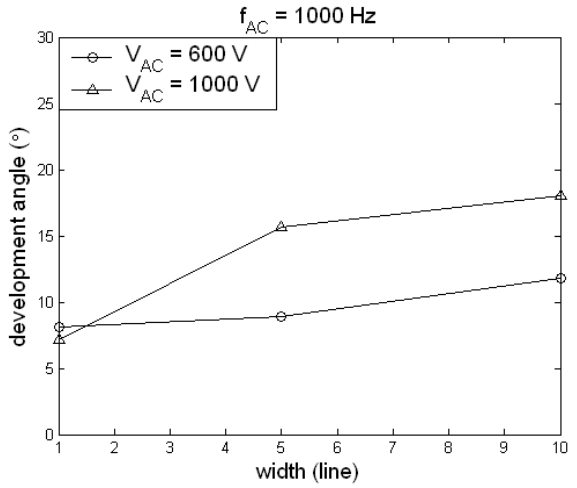

Figure 19. Critical development angle

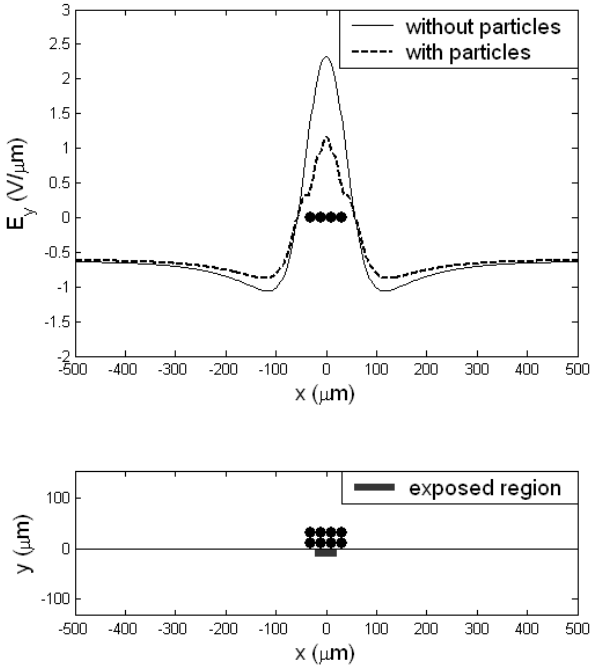

Figure 20. Normal electric field (single line) when g = 500 μm. Two layers of particles above the exposed region are shown in the bottom figure.

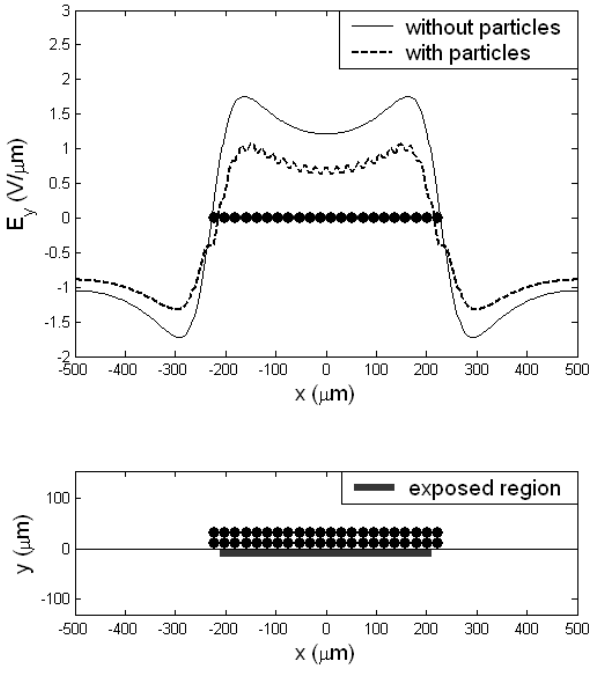

Figure 21. Normal electric field (10-pixel wide line) when g = 500 μm

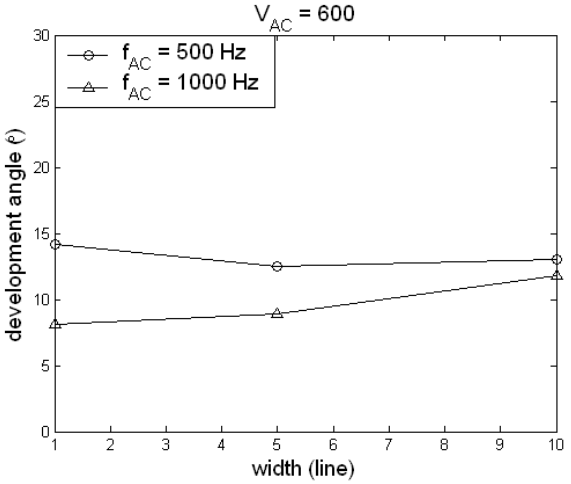

Figure 22. Critical development angle

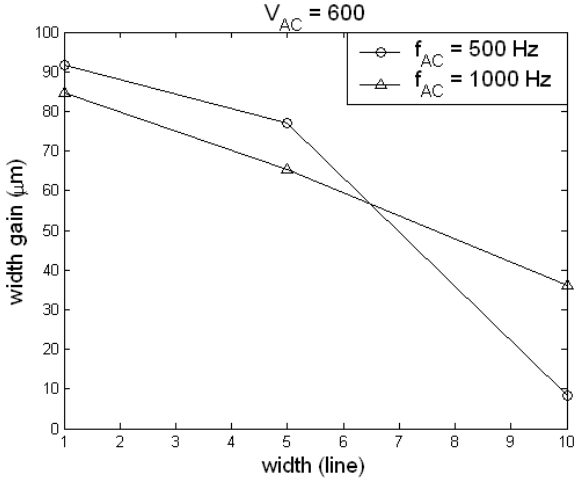

Figure 23. Developed line width gain

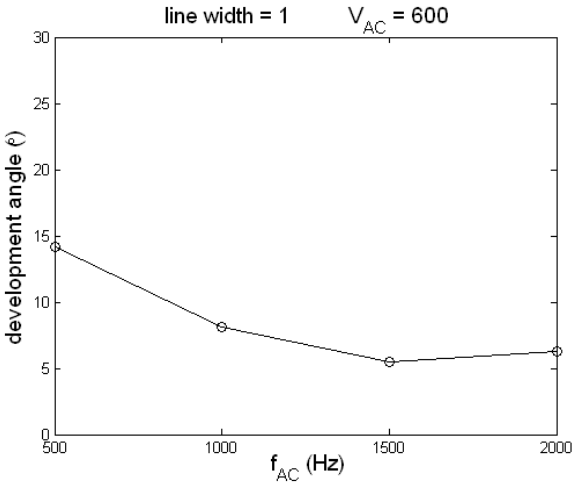

Figure 24. Critical development angle

When V_{AC} = 600 V and f_{AC} = 1000 Hz, some particles after leaving the developer surface do not quite reach the OPC surface because the AC bias changes its polarity before they do. A decrease in AC bias frequency allows some of these particles to actually reach the OPC surface and travel back to the developer. This increases the critical development angle, as shown in Fig. 22, where the frequency is reduced to 500 Hz. Although the critical development angle varies relatively little, it is noticeably larger than when f_{AC} = 1000 Hz, which resulted in an exacerbated line width gain variation, as shown in Fig. 23.

The critical development angles of the single line at frequencies 500, 100, 1500, and 2000 Hz are shown in Fig. 24. The critical development angle appears to decrease with increasing frequency and the corresponding line width gain gradually decreased from approximately 90 μm down to 80 μm.

Conclusions

A calculation procedure for simulation of toner particle movement between a cylindrical OPC and a cylindrical developer in the presence of an AC bias in non-contact, mono-component development systems was presented and simulated particle movement data using various line widths and AC bias settings were analyzed to qualitatively explain developed line width gain variations. The potential between two flat surfaces was calculated with the finite element method incorporating contributions from toner particles with a log-normal charge density distribution and then transformed into the physical geometry using conformal mapping techniques. Toner movement between the two cylindrical surfaces due to the electric field obtained from the potential was calculated using the discrete element method.

Simulated single line development showed a larger line width gain than thicker lines. It was observed that particle movement around the exposed region begins to stabilize at a certain rotation angle of the exposed region. This critical development angle, which effectively increases the air gap above the exposed region, appeared to be correlated with the input line width dependent line width gain variation. The line width gain variation was exacerbated by an increase in AC bias magnitude (severe critical development angle variation) and a decrease in AC bias frequency (relatively little critical development angle variation).

References

1. J. Yi et al., Electric Field Calculation based on PIDC in Monocomponent Development Systems, Proc. NIP-18 pg. 23-27 (2002).
2. J. Yi et al, J. Imaging. Sci. and Technol., 48:324 (2004).
3. P. A. Cundall et al., Geotechnique, 29:47 (1979).

Author Biography

Jang Yi received his B.S. degree in computer engineering from the University of Idaho in 1997 and a Ph.D. in electrical engineering from the University of Idaho in 2002. His dissertation was on modeling electrophotographic development physics. His current research area is the development process.